









Article

Crystallization Conditions and Petrogenetic Characterization of Metaluminous to Peraluminous Calc-Alkaline Orogenic Granitoids from Mineralogical Systematics: The Case of the Cambrian Magmatism from the Sierra de Guasayán (Argentina)

Priscila S. Zandomeni ^{1,2} , Juan A. Moreno ^{1,2,*} , Sebastián O. Verdecchia ^{1,2} , Edgardo G. Baldo ^{1,2} ,
Juan A. Dahlquist ^{1,2} , Matías M. Morales Cámara ^{1,2} , Catalina Balbis ^{1,2}, Manuela Benítez ³,
Samanta Serra-Varela ^{4,5}  and Carlos I. Lembo Wuest ^{1,2} 



Citation: Zandomeni, P.S.; Moreno, J.A.; Verdecchia, S.O.; Baldo, E.G.; Dahlquist, J.A.; Morales Cámara, M.M.; Balbis, C.; Benítez, M.; Serra-Varela, S.; Lembo Wuest, C.I. Crystallization Conditions and Petrogenetic Characterization of Metaluminous to Peraluminous Calc-Alkaline Orogenic Granitoids from Mineralogical Systematics: The Case of the Cambrian Magmatism from the Sierra de Guasayán (Argentina). *Minerals* **2021**, *11*, 166. <https://doi.org/10.3390/min11020166>

Academic Editor: Jarda Dostal

Received: 28 December 2020

Accepted: 31 January 2021

Published: 5 February 2021

Publisher's Note: MDPI stays neutral with regard to jurisdictional claims in published maps and institutional affiliations.



Copyright: © 2021 by the authors. Licensee MDPI, Basel, Switzerland. This article is an open access article distributed under the terms and conditions of the Creative Commons Attribution (CC BY) license (<https://creativecommons.org/licenses/by/4.0/>).

- ¹ Consejo Nacional de Investigaciones Científicas y Tecnológicas (CONICET), Centro de Investigaciones en Ciencias de la Tierra (CICTERRA), Córdoba X5016CGA, Argentina; priscilazandomeni@gmail.com (P.S.Z.); sverdecchia@unc.edu.ar (S.O.V.); edgardo.baldo@unc.edu.ar (E.G.B.); juan.andres.dahlquist@unc.edu.ar (J.A.D.); matiasmmoralesc@unc.edu.ar (M.M.M.C.); catybalbis@gmail.com (C.B.); ivan.lembow@unc.edu.ar (C.I.L.W.)
 - ² Facultad de Ciencias Exactas, Físicas y Naturales, Universidad Nacional de Córdoba, Córdoba X5016CGA, Argentina
 - ³ Comisión de Investigaciones Científicas de la Provincia de Buenos Aires (CICPBA), Instituto de Recursos Minerales (INREMI), Universidad Nacional de La Plata–CICPBA, La Plata B1904AMC, Argentina; manuelabenitez2@gmail.com
 - ⁴ Instituto de Investigación en Paleobiología y Geología, Universidad Nacional de Río Negro, Río Negro 8332, Argentina; s.serravarela@gmail.com
 - ⁵ Consejo Nacional de Investigaciones Científicas y Tecnológicas (CONICET), Ciudad Autónoma de Buenos Aires, Buenos Aires C113AAD, Argentina
- * Correspondence: jmoreno_2@ugr.es

Abstract: The Sierra de Guasayán (Eastern Sierras Pampeanas, Argentina) is formed by low to medium grade metamorphic rocks intruded by Cambrian metaluminous (La Soledad quartz-diorite), slightly peraluminous (Guasayán, El Escondido and El Martirizado granodiorite plutons), and strongly peraluminous (Alto Bello granodiorite) granitoids of the Pampean magmatic arc. Chemical compositions of amphibole, plagioclase, biotite, and titanite indicate that these granitoids were emplaced at low pressure (mostly < 3 kbar) and temperature (<770 °C) under oxidizing conditions (QFM + 1 and QFM + 2), which are similar to the emplacement conditions reported for other granites of the Pampean magmatic arc. Mineral assemblages and whole-rock and mineral chemistry of the granitoids from the Sierra de Guasayán indicate an I-type affinity for the La Soledad quartz-diorite (amphibole, biotite, and titanite), S-type affinity for the Alto Bello granodiorite (biotite, muscovite, cordierite, and sillimanite), and a hybrid nature for the main Guasayán and El Escondido plutons (biotite, monazite, and magnetite). This hybrid nature is supported by the presence of abundant mafic microgranular enclaves and rapakivi texture and by published zircon Hf-isotope data (ϵHf ; ranging from −4.76 to −0.12). This suggests, in turn, the involvement of hybridization in the genesis of these granitoids, which seems to be a common mechanism operating in the Pampean magmatic arc.

Keywords: I-type granitoids; S-type granitoids; hybrid granitoids; mineral chemistry; geothermobarometry; Sierra de Guasayán; Pampean Orogeny

1. Introduction

Granites sensu lato are the most abundant magmatic rocks of the continental crust; thus, their study represents a main topic in igneous petrology (e.g., [1–3]). Despite that they range in composition from tonalite with ca. 58 wt.% SiO_2 to alkali feldspar granite with up to ca. 80 wt.% SiO_2 (e.g., [4]), their mineralogy is relatively simple with a predominance of

quartz, plagioclase, and alkali feldspar with varying modal proportions of varietal minerals (e.g., micas, amphiboles, pyroxenes, garnet, cordierite, and aluminosilicates) and variable amounts of accessory minerals (e.g., apatite, rutile, Fe–Ti oxides, zircon, titanite, monazite, epidote, and allanite).

The study of these major and accessory minerals can be used to assess the geochemical affinities of the host granitoids (e.g., I- or S-type signature) as well as to establish their crystallization/emplacement conditions. For instance, the typical main mineral assemblage of metaluminous to slightly peraluminous, calc-alkaline I-type granites commonly presents hornblende and biotite with titanite, epidote, and magnetite as the main accessory minerals (e.g., [5–7]), whereas muscovite and biotite along with other aluminous minerals (e.g., cordierite, garnet, andalusite/sillimanite/kyanite, etc.) are widely recognized in S-type granites, in which monazite and ilmenite are the most common accessory minerals (e.g., [5–8]). In addition, the chemical composition of certain minerals (e.g., pyroxene, amphibole, and biotite) can be used to infer the nature of the crystallizing magma (e.g., alkaline, calc-alkaline, and peraluminous character) (e.g., [9–14]). Furthermore, mineral chemistry is an important tool to estimate crystallization parameters of granitic magmas. In this regard, several geobarometers and geothermometers based on amphibole, amphibole-plagioclase, biotite, and titanite compositions are widely used in the literature (e.g., [15–24]), whilst the oxygen fugacity of the magmas can be roughly estimated using Fe/(Fe + Mg) ratios of amphibole and biotite (e.g., [25–27]).

In this work, we present chemical data of major minerals and thermobarometric calculations for several early Cambrian granitoids and mafic enclaves from the Sierra de Guasayán (Eastern Sierras Pampeanas of Argentina), which range from quartz-diorite to monzogranite. The main goal of this work is to constrain the crystallization conditions of these magmas and to characterize their mineralogy, highlighting chemical differences among the minerals of the various granitoids, in order to contribute to the understanding of their petrogenesis. Notably, in this work, we show that the hybrid nature of granitoids of the Guasayán pluton, as revealed by zircon Hf isotopes, is properly recognized from mineral chemistry. In addition, this work reports the first mineral data set for granitoids of the Pampean magmatic arc that is accessible to the international geology community, the previous data were mainly presented in contributions to congresses, and allowed us to determine their *P-T* crystallization conditions.

2. Geological Setting and Geology of the Sierra de Guasayán

The Sierra de Guasayán is located in the Sierras Pampeanas region (central and northwestern Argentina), where the exposed basement blocks were uplifted during the Andean Orogeny in the modern 26–33° S flat-slab segment of the Nazca plate up to 900 km away from the trench ([28] and references therein). The Sierras Pampeanas were subdivided into Western and Eastern Sierras Pampeanas according to their dominant lithologies [29]. The Western Sierras Pampeanas are dominated by 1030–1330 Ma (“Grenville orogen”) igneous and metamorphic rocks, intruded by relatively scarce Ordovician granites of the Famatinian cycle and a few Early Carboniferous plutons (e.g., [30–34] and references therein). The Eastern Sierras Pampeanas are characterized instead by a low- to high-grade Late Ediacaran to Early Palaeozoic basement, intruded by voluminous granitic batholiths and plutons of Early Cambrian (Pampean), Early Ordovician (Famatinian), Middle-Late Devonian (Achalían), and Carboniferous (Early Gondwana) age ([34–37] and references therein). The Early Cambrian magmatism recognized in the Eastern Sierras Pampeanas and the Cordillera Oriental of NW Argentina belongs to the Pampean magmatic arc (e.g., [38–44] and references therein), which formed part of the much greater Terra Australis Orogen developed in the West Gondwana margin [45].

The Sierra de Guasayán, included in the Eastern Sierras Pampeanas morphotectonic unit (Figure 1), is located in the western Santiago del Estero province (Argentina), close to the boundary with the Catamarca province, and is an N–S elongated mountain range 75 km long and 2 km wide (Figures 1 and 2). It mainly consists of Ediacaran–Early Cambrian

metamorphic and igneous rocks corresponding to the Pampean orogen and subordinate Mesozoic volcanic and sedimentary rocks, and Quaternary sediments [43,46–52]. The metasedimentary country rocks are low-grade metapsammites, phyllites, and subordinate calc-silicate rocks in the northern segment of the Sierra de Guasayán, whereas garnet-bearing schists and quartz-mica schists crop out in the southern segment. These metasedimentary rocks are considered equivalent to the rocks from the thick (>2000 m) Puncoviscana Series (e.g., [35]). The Puncoviscana Series was originally defined by Turner [53] (Puncoviscana Formation) from the type section in northwestern Argentina where it consists of a very low-grade marine metasedimentary succession, deposited in the Late Ediacaran ([43,54] and references therein), but mainly in the Early Cambrian, and folded still within the Early Cambrian (537–523 Ma; [55] and references therein). Based on detrital zircon age-patterns, the Puncoviscana Series is widely recognized in the high-grade metasedimentary basement of the Eastern Sierras Pampeanas [35,43]. In the Sierra de Guasayán, the metamorphic basement is intruded by subcircular igneous bodies like the El Escondido and El Martirizado plutons and by the elongated Cambrian Guasayán pluton (533 ± 4 Ma; [42]) (Figure 2). In addition, small isolated granitoid bodies such as the La Soledad quartz-diorite and the Alto Bello two mica granodiorite crop out within the larger Guasayán pluton (Figure 2).

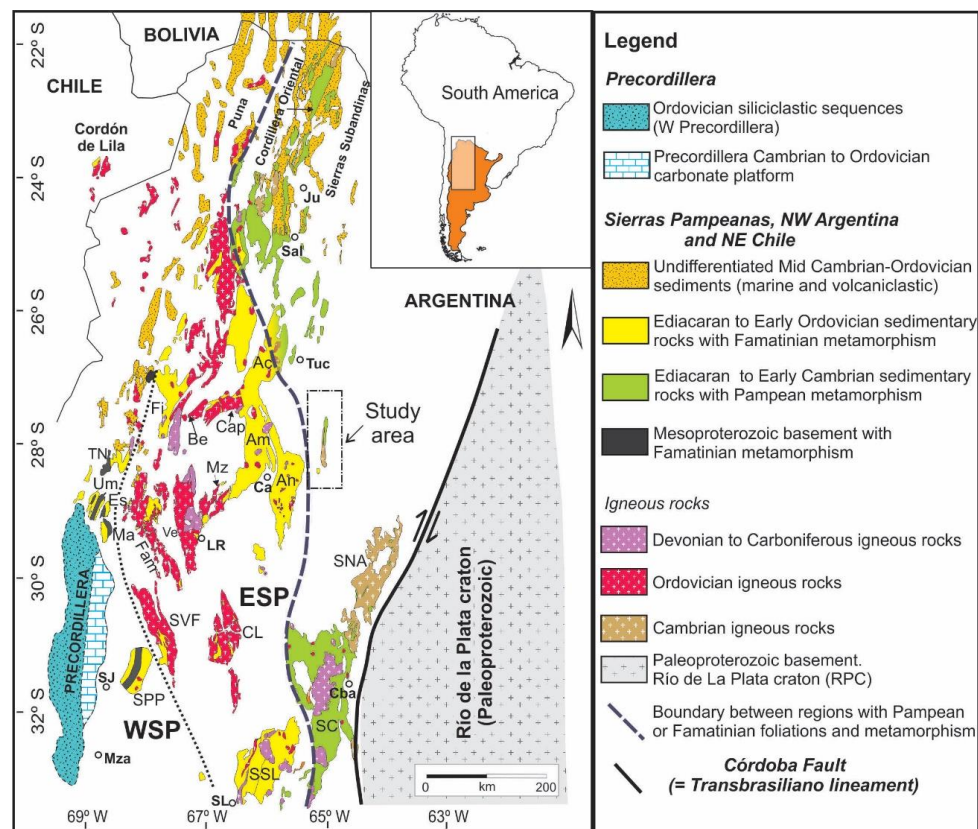


Figure 1. Early Paleozoic geology of the Sierras Pampeanas, Puna, Cordillera Oriental and Sierras Subandinas. EPEB: Eastern Puna Eruptive Belt. Main ranges are indicated: Sierra de Aconquija (Ac), Sierra de Ambato (Am), Sierra de Ancasti (An), Sierra de Belén (Be), Sierra de Capillitas (Cap), Sierra del Espinal (Es), Sierra de Famatina (Fam), Sierra de Fambalá (Fi), Sierras de Chepes-Los Llanos (CL), Sierra de Maz (Ma), Sierra de Mazán (Mz), Sierra de Córdoba (SC), Sierra Norte-Ambargasta (SNA), Sierra de Pie de Palo (SPP), Sierra de San Luis (SSL). Sierra del Toro Negro (TN), Sierra de Valle Fértil (SVF), Sierra de Velasco (Ve), Sierra de Umango (Um). Town localities: Jujuy (Ju), Salta (Sal), Tucumán (Tuc), Catamarca (Ca), La Rioja (LR), San Juan (SJ), Córdoba (Cba), Mendoza (Mza), San Luis (SL). Modified from Rapela et al. [37].

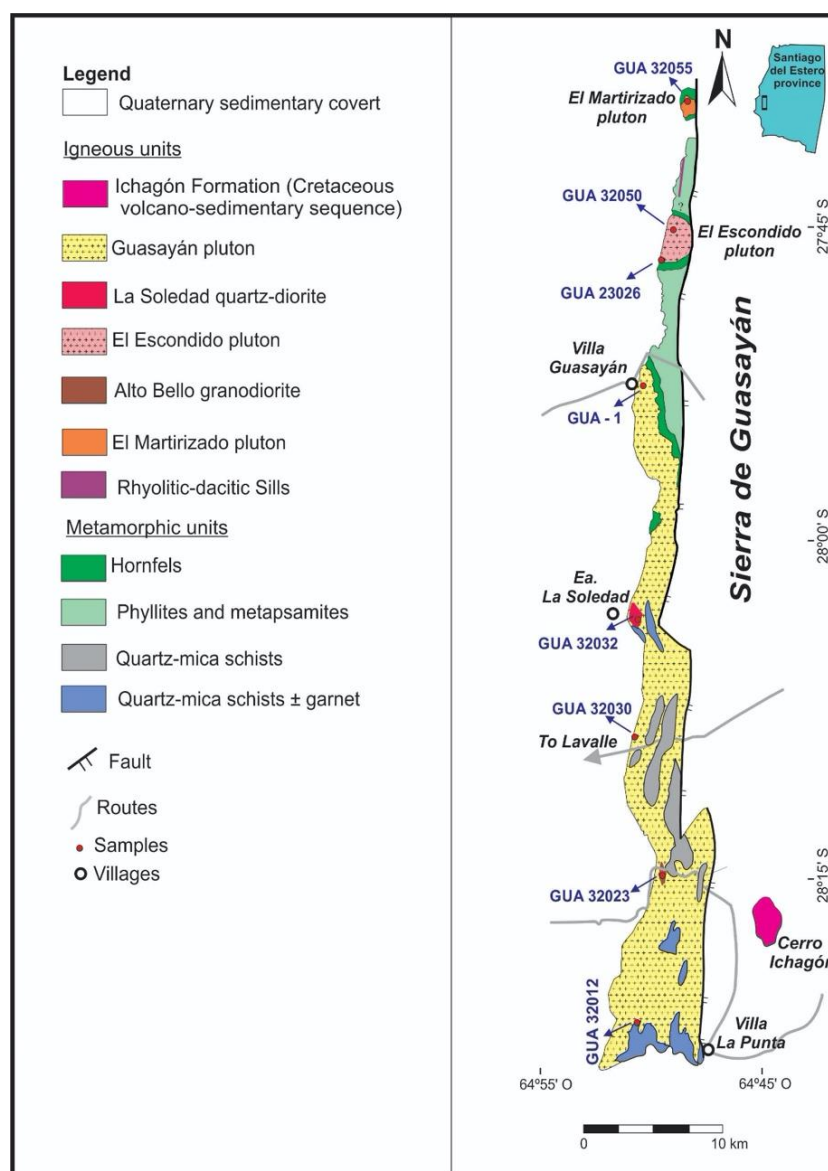


Figure 2. Geological sketch of the Sierra de Guasayán with location of the studied samples. Location of sample GUA-1 from Dahlquist et al. [43] is also indicated.

Geochemical Considerations

Although still scarce, some geochemical data for the plutons of the Sierra de Guasayán have been reported by Dahlquist et al. [43] and Zandomeni et al. [56]. According to this, the granitoids from the Sierra de Guasayán show a range of silica contents between 56.8 wt.% and 69.2 wt.% [43,56], with the Guasayán pluton showing the most felsic compositions and the La Soledad quartz-diorite the most basic. They are mainly calc-alkalic and magnesian granitoids, showing typical compositions of granitic rocks related to an active continental margin. The main differences appear when the alumina saturation index ($ASI = \text{molar } Al_2O_3 / (CaO + Na_2O + K_2O)$) is taken into account, with the La Soledad quartz-diorite being clearly metaluminous ($ASI = 0.8$), whereas samples from the Guasayán and El Escondido plutons are weakly peraluminous ($ASI = 1.05\text{--}1.11$) and the Alto Bello granodiorite is strongly peraluminous ($ASI = 1.49$). Despite some overlap, samples from the Guasayán pluton ($ASI = 1.05\text{--}1.11$) are slightly more peraluminous than those from the El Escondido pluton ($ASI = 1.06\text{--}1.08$).

Granitoids from the Sierra de Guasayán are similar to the granites of the Pampean magmatic arc from the Sierra Chica de Córdoba [38] and the Sierra Norte-Ambargasta

batholith [41,57], that can be considered equivalents [43]. This is also supported by the Cambrian age of 533 ± 4 Ma obtained by Dahlquist et al. [43] for a granodiorite sample from the Guasayán pluton. Furthermore, these geochemical data for the Cambrian magmatism of the Sierra de Guasayán suggest they represent a spatial link between the Cambrian igneous units from the Sierra Norte-Ambargasta (Córdoba and Santiago del Estero provinces) and those from the Tastil batholith in the Cordillera Oriental (Salta) [40]. Therefore, the available data suggest that the granitoids from the Sierra de Guasayán were part of the Pampean magmatic arc (540–520 Ma), which was active during the construction of the western margin of Gondwana (e.g., [43]).

3. Samples and Methods

For this study, 25 samples of granitic rocks were collected and studied petrographically. Mineral compositions were determined in seven samples: one granodiorite from the Guasayán pluton (GUA 32012), one mafic enclave from the Guasayán pluton (GUA 32030), one sample from the La Soledad quartz-diorite (GUA 32032), one monzogranite from the El Escondido pluton (GUA 32050), one mafic enclave from the El Escondido pluton (GUA 23026), one granitic sample from the El Martirizado pluton (GUA 32055) and one sample from the Alto Bello two mica granodiorite (GUA 32023). In addition, published compositions of plagioclase, alkali feldspar, and biotite from a granodiorite of the Guasayán pluton (sample GUA-1 from [43]) have also been included in figures and descriptions.

Mineral compositions were determined by wavelength-dispersive spectrometry (WDS) with a JEOL JXA-8230 electron microprobe equipped with three WDS spectrometers at Electron Microscopy Laboratory and X-ray Analyses unit of Córdoba National University (<http://www.famaf.unc.edu.ar/lamarx/lamerx1sem.html>). Operating conditions were: acceleration voltage of 15 kV, probe current of 10 nA in phyllosilicates, and 20 nA in nominally anhydrous minerals. A beam diameter ranging from 5 to 8 μm with a count time of 10 s at its peak, and 5 s at each background position. In order to minimize migration effects in Na and K, these elements were analyzed first in each analytical run, 5 s on peak and 2.5 s on the background. Synthetic and natural mineral standards were used as internal calibrations: Si (forsterite, albite, anorthoclase, diopside, and wollastonite), K (orthoclase) Al (anorthite and albite), Fe (hematite), Mg (forsterite and MgO), Na (albite and anorthoclase), Mn (pyrolusite), Ti (ilmenite, titanite, and Ti), Sr (celestine), Ba (baryte), Cr (chromite), Ca (anorthite and diopside), P (libethenite), F (topaz), Cl (sodalite) and Zn (ZnO). The analyses were corrected using the Phi-Rho-Z method. Mineral names were abbreviated following Whitney and Evans [58]. The different mineral analyses are listed in Table S1 (Supplementary Materials). Corrected element contents were converted to oxides assuming stoichiometry; FeO represents “total iron”. Mineral compositions are expressed in weight percent (wt.%) of the main element oxides, and are recast into numbers of cations in atoms per formula units (apfu) following recommendations by Papike [59,60] and Deer et al. [61]. Structural formulas of muscovite and biotite were normalized to 22 oxygens [62], plagioclase and K-feldspar to eight oxygens [63], and amphibole to 23 oxygens. For description and classification purposes, amphibole structural formulas were calculated according to [64], following the IMA12 recommendations and normalizing to the sum of cations from Si to Ca (including Li) = 15 and from Si to Mg (including Li) = 13, with the Fe^{3+} calculated according to [65]. For thermobarometric calculations, amphibole formulas and $\text{Fe}^{3+}/\text{Fe}^{2+}$ ratios were determined assuming 13 cations exclusive of Ca, Na, and K (13-CNK method; [66]) on the basis of 23 oxygen atoms. It should be noted that for the new amphibole-plagioclase thermometers from Molina et al. [22], amphibole formulas were also calculated on the basis of 23 oxygens but with ferric/ferrous iron ratios calculated by charge balances and stoichiometric constraints according to [67].

4. Field Relations and Petrography

4.1. The Guasayán Pluton

The Guasayán pluton is an undeformed granitoid body that crops out over an area of approximately 170 km². The contact with the country rock is sharp and shows the development of cordierite-biotite-K-feldspar hornfels. It contains metamorphic septa (10–30 m long) and rounded mafic microgranular enclaves (MME; 5–10 cm in diameter) (Figure 3A). Centimetric biotite clots and subangular metamorphic xenoliths are recognized. Plagioclase-mantled K-feldspar phenocrysts (rapakivi texture) have been observed (Figure 3B). The Guasayán pluton is mainly made of porphyritic biotite medium-grained grey granodiorites to monzogranites with K-feldspar phenocrysts (3.0 cm × 1.5 cm to 2.0 cm × 1.0 cm) set in an equigranular matrix composed of plagioclase, quartz, alkali feldspar, and biotite (Figure 3C). K-feldspar phenocrysts define a preferred orientation and a dominant N–S magmatic foliation. Zircon, apatite, monazite, ilmenite, and magnetite are accessory minerals. Chlorite, fine-grained white mica aggregates (“sericite”), and epidote are common secondary minerals.

Under the petrographic microscope, two main varieties of plagioclase were recognized (coarse-grained: 8.0 mm × 5.0 mm; medium-grained: ranging from 5.0 mm × 2.0 mm to 2.0 mm × 1.2 mm). Both varieties display subhedral crystal shape, with concentric compositional zoning, polysynthetic twinning, and common inclusions of biotite and Fe-Ti oxides. Myrmekites are occasionally observed in contact with K-feldspar. This latter can also be grouped into two families: a) coarse-grained (3.0 cm × 1.5 cm to 2.0 cm × 1.0 cm) perthitic phenocrysts; b) medium-grained (3.0 mm × 1.5 mm to 4 mm × 2 mm) subhedral to anhedral crystals that commonly occur in interstitial position. Microcline twinning is common, and some crystals show perthitic texture. Biotite, plagioclase, and quartz are common inclusions in K-feldspar. Biotite shows subhedral to anhedral forms with sizes ranging between 2 mm × 1 mm to 1 mm × 0.5 mm and containing inclusions of zircon, apatite, and quartz.

The mafic enclaves are equigranular and fine-grained with quartz-dioritic to granodioritic composition and formed by plagioclase, quartz, biotite ± poikilitic amphibole as main minerals and ilmenite, epidote, zircon, and apatite as accessory minerals.

4.2. The El Escondido Pluton

The El Escondido pluton crops out at the north of Sierra de Guasayán as a small subcircular body of ~6.23 km² (Figure 2). It is emplaced discordantly in the metamorphic basement, developing a thin metamorphic aureole with cordierite-biotite-K-feldspar hornfels. It contains abundant rectangular metamorphic xenoliths (20–30 cm long) and rounded microgranular mafic enclaves (<40 cm in diameter) (Figure 3D). It is an equigranular medium-grained grey granodiorite composed of plagioclase, quartz, alkali feldspar, and biotite, with allanite, monazite, zircon, apatite, and magnetite as accessory minerals (Figure 3E). Porphyritic facies with phenocrysts of plagioclase (1–2 cm) and alkali feldspar (~5 cm) is found in the border of the pluton. Porphyritic facies has a rapakivi texture represented by K-feldspar phenocrysts with a plagioclase rim (Figure 3F).

Plagioclase is subhedral, medium-grained (1.5–2 mm × 0.7–1 mm) with polysynthetic twinning and compositional zoning and can show inclusions of biotite and Fe-Ti oxides. The porphyritic facies has plagioclase phenocrysts with sizes up to 3 mm × 2 mm to 2 mm × 1 mm. K-feldspar is subhedral medium-grained (2.5–2 mm × 1.5–0.7 mm) with microperthitic intergrowths and Carlsbad twinning. It commonly presents inclusions of biotite, plagioclase, and quartz. In the porphyritic facies, K-feldspar phenocrysts (3 mm × 1.5 mm to 2.5 mm × 1.8 mm) are subhedral with perthitic intergrowths, microcline, and Carlsbad twinning and inclusions of biotite, quartz, and plagioclase. Biotite is subhedral to anhedral, with sizes between 1 mm × 0.4 mm and 0.7 mm × 0.5 mm and abundant inclusions of apatite and zircon.

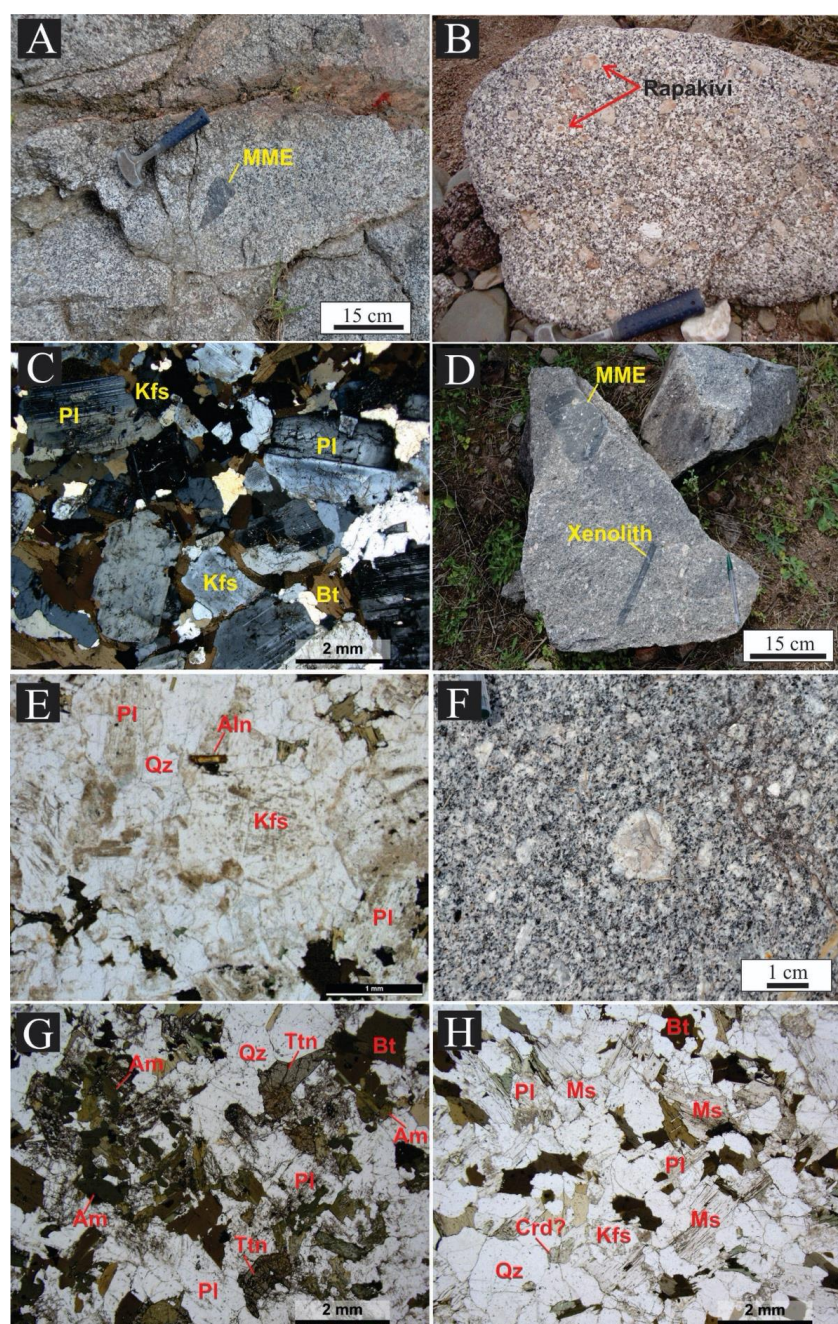


Figure 3. Field photographs and photomicrographs of the granitoids from the Sierra de Guasayán. (A) Outcrop of a porphyritic granitoid from the Guasayán pluton with centimeter-scale mafic micro-granular enclaves (MME). (B) Block of a porphyritic granitoid (Guasayán pluton) showing K-feldspar phenocrysts mantled by plagioclase (rapakivi texture). (C) Plagioclase, quartz, K-feldspar, and biotite of the medium-grained equigranular matrix from a granodiorite of the Guasayán pluton. (D) Centimeter-scale MME and metamorphic xenoliths in the El Escondido pluton. (E) Plagioclase, K-feldspar, quartz, biotite, and allanite in the equigranular facies of the El Escondido pluton. (F) Possible rapakivi texture in the porphyritic facies of the El Escondido pluton. (G) Plagioclase, quartz, biotite, amphibole, and titanite from the medium-grained equigranular La Soledad quartz-diorite. (H) Quartz, plagioclase, K-feldspar, biotite, primary muscovite, and pinite pseudomorphs after cordierite from the medium-grained equigranular Alto Bello granodiorite. Mineral abbreviations: amphibole (Am), biotite (Bt), plagioclase (Pl), K-feldspar (Kfs), quartz (Qz), allanite (Aln), cordierite (Crd), titanite (Ttn), and muscovite (Ms).

The mafic enclaves are roughly equigranular and fine- to medium-grained with tonalitic to granodioritic composition, mainly consisting of plagioclase, quartz, biotite, and amphibole. The accessory mineral assemblage is made up of zircon, apatite, ilmenite, epidote, and allanite.

4.3. The El Martirizado Pluton

The El Martirizado pluton crops out in the northernmost sector of the Sierra de Guasayán (Figure 2) as an undeformed red igneous body with an exposed area of $\sim 0.6 \text{ km}^2$ and diffuse contacts with the country rock. Vegetation and soil development hinders the observation of field relations. It is an equigranular medium- to fine-grained granodiorite to monzogranite composed of plagioclase, quartz, alkali feldspar, and biotite with monazite, zircon, apatite, and rutile as accessory minerals. Chlorite, magnetite, calcite, and fine-grained white mica aggregates are secondary minerals. Metamorphic xenoliths and mafic microgranular enclaves have not been observed.

Plagioclase is subhedral, fine-grained ($0.6 \text{ mm} \times 0.3 \text{ mm}$), with polysynthetic twinning and compositional zoning, and containing scarce biotite inclusions. K-feldspar is subhedral, fine-grained ($0.5 \text{ mm} \times 0.3 \text{ mm}$) with microperthitic intergrowths. Biotite is subhedral and fine-grained ($0.4 \text{ mm} \times 0.2 \text{ mm}$), with inclusions of zircon and apatite.

4.4. The La Soledad Quartz-Diorite

The La Soledad quartz-diorite occurs as several isolated rounded blocks covering an area of about 200 m^2 and surrounded by the porphyritic biotite Guasayán pluton, although contacts between them could not be observed. It is an equigranular medium to fine-grained grey quartz-diorite composed of plagioclase, quartz, biotite, calcic amphibole, and alkali feldspar (Figure 3G). The accessory mineral assemblage consists of titanite, zircon, apatite, and ilmenite. Common secondary minerals are chlorite, epidote, and fine-grained white mica aggregates.

Plagioclase is medium-grained ($1.0\text{--}1.8 \text{ mm} \times 0.4\text{--}0.7 \text{ mm}$), mostly subhedral with polysynthetic twins and compositional zoning. Biotite, apatite, and Fe-Ti-oxide are common inclusions in plagioclase. Biotite is subhedral with sizes around $0.5\text{--}1.5 \text{ mm} \times 0.2\text{--}0.5 \text{ mm}$, and some crystals show abundant inclusions of Fe-Ti oxides and apatite and scarce inclusions of amphibole. Primary titanite is euhedral to subhedral, with variable sizes between $0.5\text{--}1.8 \text{ mm}$ long, whereas a secondary variety is recognized, forming coronas around opaque minerals (likely ilmenite). Amphibole is euhedral to subhedral with sizes around $0.5\text{--}1.5 \text{ mm} \times 0.2\text{--}0.7 \text{ mm}$. It has inclusions of apatite and Fe-Ti oxides. K-feldspar appears as scarce and anhedral crystals ($<1 \text{ mm}$) with microcline twinning in an interstitial position.

4.5. The Alto Bello Granodiorite

The Alto Bello granodiorite crops out in the southern segment of the Sierra de Guasayán as numerous isolated blocks exposed in a small area of $\sim 500 \text{ m}^2$ and surrounded by the porphyritic biotite Guasayán pluton to the east (Figure 2), although the contact was not observed. To the west, the outcrops are totally covered by vegetation and soils. It is an equigranular, fine- to medium-grained two mica grey granodiorite that exhibits internal mica foliation with abundant metamorphic xenoliths oriented parallel to it. The major mineral assemblage consists of plagioclase, quartz, alkali feldspar, biotite, muscovite, cordierite, and sillimanite with monazite, zircon, apatite, ilmenite, and rutile as accessory minerals (Figure 3H). Chlorite, pinite, epidote, and fine-grained white mica aggregates are common secondary phases.

Plagioclase is subhedral, fine-grained ($0.8\text{--}1.3 \text{ mm} \times 0.5 \text{ mm}$) with polysynthetic twinning and compositional zoning. K-feldspar is anhedral with sizes between 0.7 and 1 mm and occasionally reaching up to 2.5 mm . It does not show twinning nor perthite. Muscovite is subhedral, medium-grained ($1\text{--}1.5 \text{ mm} \times 0.5\text{--}1.5 \text{ mm}$) with inclusions of sillimanite (fibrolite). Biotite is subhedral with zircon inclusions and variable sizes around

1–2 mm × 0.5–1 mm. Cordierite appears as pseudomorphs of pinite and disoriented white mica aggregates.

5. Mineral Chemistry

5.1. Plagioclase

Plagioclase in the granodiorites of the Guasayán pluton varied from andesine to oligoclase (An_{20–47}) (Figure 4) with cores (An_{32–47}) richer in CaO than rims (An_{20–27}) (Table S1). The plagioclase of smaller size (~2 mm) was oligoclase with a homogeneous composition (An_{20–22}), similar to that of the rims of the bigger plagioclase crystals (Table S1). Plagioclase in the mafic enclave (GUA 32030) was richer in calcium than the plagioclase from the host rock, ranging between andesine and labradorite (Figure 4) with cores of An_{56–60} and rims of An_{34–44} (Table S1).

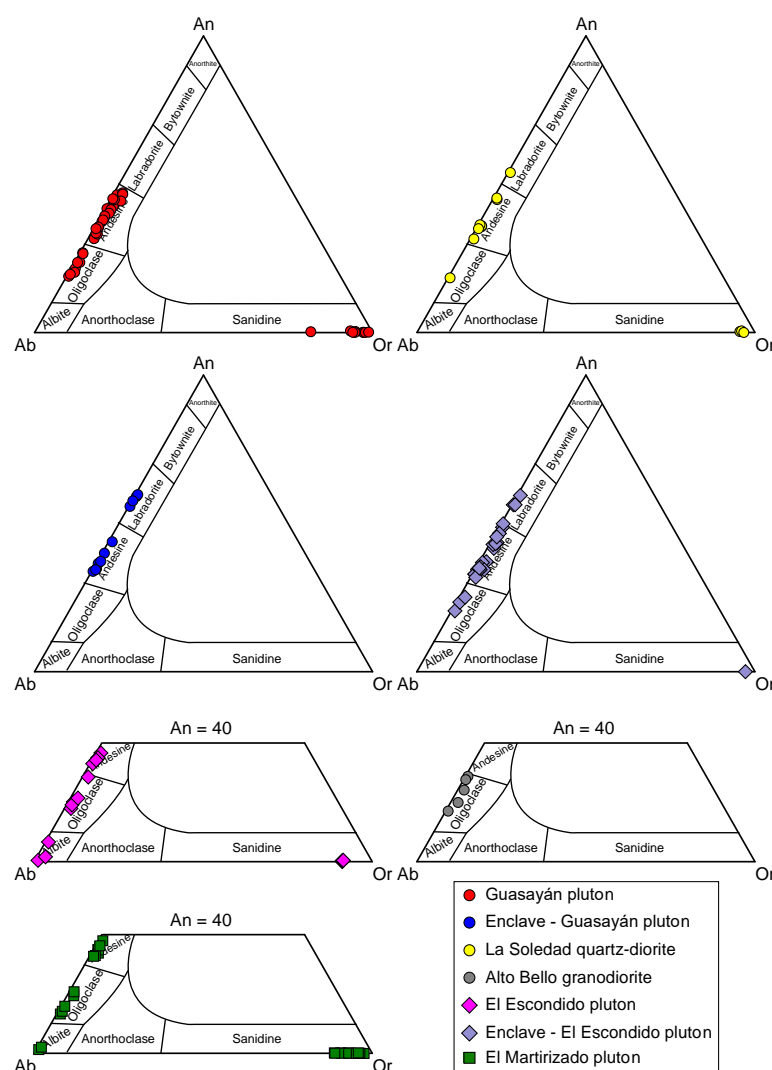


Figure 4. Composition of feldspars from the granitoids of the Sierra de Guasayán. An–Ab–Or diagram (data in mol%). Abbreviations: Ab, albite; An, anorthite; Or, orthoclase.

Plagioclase from the El Escondido pluton showed cores of andesine (An_{33–37}) and rims of oligoclase (An_{18–29}) that occasionally had an external rim of albite (Ab_{92–99}) (Figure 4; Table S1). Plagioclase in the mafic enclave (GUA 23026) had more calcic compositions than the host rock, varying between oligoclase and labradorite (Figure 4) with a core rich in Ca (An_{49–59}), surrounded by a shell of andesine (An_{33–43}) and an external rim of oligoclase (An_{20–25}) (Table S1).

In the La Soledad quartz diorite, plagioclase showed a core of andesine-labradorite composition (An_{45-54}) surrounded by a shell of sodic andesine (An_{30-37}) and a fine external rim of oligoclase (An_{18}) (Figure 4) (Table S1). In a granodiorite of the El Martirizado pluton it showed andesine composition in the cores (An_{33-38}) with rims of oligoclase (An_{13-21}) and a fine external rim of albite (Ab_{97-98}) (Figure 4; Table S1). Finally, plagioclase from the Alto Bello granodiorite was less calcic than those from the other granitic bodies, showing oligoclase compositions (Figure 4) with cores slightly richer in Ca (An_{24-29}) than rims (An_{17-20}) (Table S1).

5.2. Alkali Feldspar

Alkali feldspar from the studied samples had a sanidine composition with orthoclase contents varying between 80 and 99 (94 ± 4) (Figure 4; Table S1).

5.3. Amphibole

The amphibole in the La Soledad quartz-diorite was mainly ferro-pargasite to ferro-hornblende (Figure 5A) with $Mg/(Mg + Fe^{2+})$ of 0.44–0.54 and Ti and Al^{total} contents of 0.07–0.27 apfu and 1.34–1.63 apfu, respectively (Table S1).

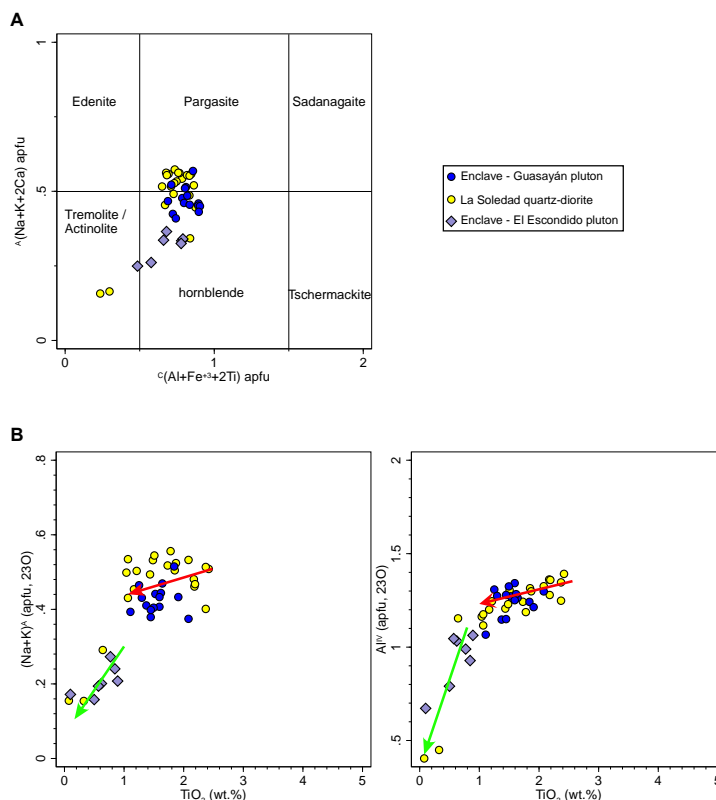


Figure 5. Composition of amphiboles from the granitoids of the Sierra de Guasayán. (A) Amphibole classification diagram of [65]. (B) $(Na + K)^A$ vs. TiO_2 and Al^{IV} vs. TiO_2 diagrams. Red arrows show primary trends and green arrows secondary trends from [14]. apfu: atoms per formula units.

Amphibole from the mafic enclave of the Guasayán pluton (GUA 32030) also varied between ferro-ferri-hornblende and ferro-pargasite but with a predominance of the hornblendic compositions (Figure 5A), showing $Mg/(Mg + Fe^{2+})$ of 0.45–0.48, Ti contents of 0.13–0.24 and Al^{total} contents ranging from 1.25 to 1.41 (Table S1), which were similar to those of the La Soledad quartz-diorite.

In the mafic enclave from the El Escondido pluton (GUA 23026), amphibole was magnesio-ferri-hornblende with roughly homogeneous $Mg/(Mg + Fe^{2+})$ values of 0.60–0.65 that were higher than those from the other studied samples, which may indicate more oxi-

dant conditions for this sample (e.g., [68,69]). In addition, this sample had Ti (0.01–0.10 apfu) and Al^{total} (0.86–1.21 apfu) contents that are lower than those from the other two samples.

Molina et al. [14] differentiated amphibole primary and secondary trends as a function of the TiO_2 content of amphibole and established that low TiO_2 , Al^{IV} and $(\text{Na} + \text{K})^{\text{A}}$ in amphibole are indicative of low-temperature subsolidus reequilibration. The studied compositions could be divided into clearly differentiated groups and/or trends (Figure 5B), similar to those shown by Molina et al. [14]. According to this, all compositions with $\text{TiO}_2 < 1$ wt.% correspond to amphiboles that underwent subsolidus reequilibration.

5.4. Trioctahedral Mica

Biotite in most of the studied samples had a dominantly annite composition (Figure 6A), except the mica from the Alto Bello granite that was siderophyllite to high-Al annite and one analysis from sample GUA 32030 (mafic enclave from the Guasayán pluton) with siderophyllite composition (Figure 6A). The less magnesian mica is that from the Guasayán pluton with atomic $\text{Mg}/(\text{Mg} + \text{Fe}^{\text{total}})$ of 0.34–0.37 (Table S1), whereas the rest of the studied micas have variable $\text{Mg}/(\text{Mg} + \text{Fe}^{\text{total}})$ values that range between 0.39 and 0.54 (Table S1). The Al^{total} contents of the studied micas varied between 2.47 and 3.51 apfu (Table S1), with the La Soledad quartz-diorite showing the lowest values (2.47–2.62 apfu) and the Alto Bello granodiorite the highest (3.43–3.51 apfu), which is in accordance with the presence of primary muscovite in the latter as described below. Calculated mica Li contents using empirical expressions derived by Tischendorf et al. [70] were low, with the Guasayán pluton reaching maximum values of ~ 0.13 apfu (Table S1). Fluorine contents were also low (0.34 ± 0.18 wt.%).

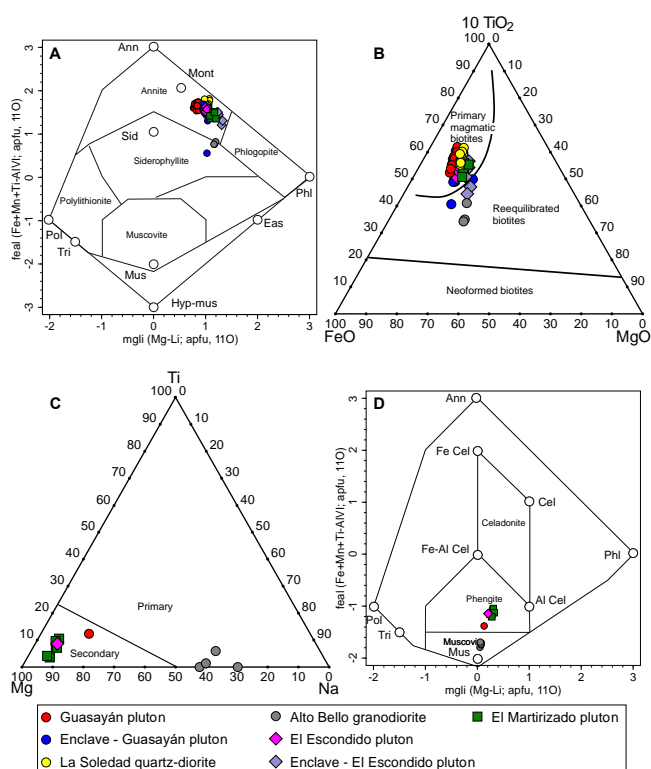


Figure 6. Composition of micas from the granitoids of the Sierra de Guasayán. (A) Feal vs. mgli diagram (after [71]). (B) 10 TiO_2 –FeO–MgO ternary diagram from [72]. (C) Atomic Ti–Na–Mg diagram with compositional fields for primary and secondary micas from [73]. (D) Feal vs. mgli diagram for white mica (after [70]). Abbreviations: Ann, annite; Cel, celadonite; Eas, eastonite; Hyp-mus, hyper-muscovite; Mus, muscovite; Mont, montdorite; Phl, phlogopite; Pol, polyolithionite; Sid, siderophyllite; Tri, trilithionite.

In the TiO_2 –FeO–MgO diagram of Nachit et al. [72], most of the analyses plotted in the field of the primary magmatic biotites (Figure 6B), although biotite from the Alto Bello granodiorite seems to have undergone certain degree of reequilibration, since they plotted in the field of the reequilibrated biotites (Figure 6B). However, this latter has Al^{VI} values of 0.8–0.9 apfu that were slightly lower than typical values of reequilibrated and neoformed biotites ($\text{Al}^{\text{VI}} > 1$ apfu; [72]), suggesting that the reequilibration process did not change that much the composition of this biotite. TiO_2 content of this biotite was low (<2 wt.%), also suggesting it was in a late crystallizing phase.

5.5. Dioctahedral White Mica

Primary white mica (Figure 6C) from sample GUA-32023 of the Alto Bello granodiorite was muscovite (Figure 6D) with relatively high Na contents (0.2–0.28 apfu), low Ti (<0.02 apfu), low F (0.08–0.21 wt.%), and $\text{Mg}/(\text{Mg} + \text{Fe}^{\text{total}})$ values of 0.38–0.42 (Table S1). On the other hand, secondary mica (Figure 6C) from the Guasayán, El Escondido, and El Martirizado plutons showed fengitic compositions (Figure 6D).

5.6. Titanite

Titanite was only present in the La Soledad quartz-diorite and is characterized by 37–40 wt.% TiO_2 , 27–30 wt.% CaO, 1–2 wt.% Al_2O_3 , and 0.5–2.8 wt.% FeO (Table S1). It showed Fe/Al values mostly ranging between 0.5 and 1.4, which are typical of silica-saturated igneous rocks [74]. Only three analyses had lower Fe/Al values (0.22–0.37), suggesting a likely secondary origin.

6. *P-T* and *fO₂* Estimations

Crystallization conditions for the different granitoids from the Sierra de Guasayán were determined from the chemical analyses of amphibole, plagioclase, biotite and titanite, using the following thermobarometric expressions: (1) total Al in biotite barometer [17] (uncertainty: ± 0.33 kbar); (2) Al_2O_3 in titanite barometer [20] (uncertainty: ± 0.6 to 1.0 kbar); (3) Al-in-amphibole barometer from Mutch et al. [23] (uncertainty: ± 0.5 kbar); (4) amphibole-plagioclase barometer [21] (uncertainty: ± 1.5 to 2.3 kbar); (5) Ti-Amphibole thermometer from Liao et. al. [24] (uncertainty: ± 35 °C); and (6) amphibole-plagioclase thermometers from Holland and Blundy [16] (expression A; uncertainty: ± 40 °C) and Molina et al. [22] (expressions A1, A2 and B2; uncertainty: ± 25 –30 °C).

In the next subsections, means of the obtained pressure and temperature estimates are given along with their respective standard deviation, which is always lower than the uncertainty of the methods, indicating that the compositional variability of the analyses was low. However, the real uncertainty is from the applied method.

6.1. Pressure Estimations

The barometer based on the Al content of biotite gave low crystallization pressures that ranged between 1.0 and 2.1 kbar (Tables S1 and S2, Supplementary Materials) for most of the studied samples, being 2.0 ± 0.1 kbar (range: 1.8–2.1 kbar) in the Guasayán pluton, 1.7 ± 0.3 kbar (range: 1.4–2.1 kbar) in the mafic enclave from the Guasayán pluton, 1.7 ± 0.1 kbar (range: 1.5–1.8 kbar) in the El Escondido pluton, 1.1 ± 0.1 kbar (range: 1.0–1.3 kbar) in the mafic enclave of the El Escondido pluton, 1.2 ± 0.1 kbar (range: 1.0–1.4 kbar) in the La Soledad quartz-diorite and 1.8 ± 0.2 kbar (range: 1.5–2.1 kbar) in the El Martirizado pluton.

The titanite barometer also yielded low pressures of 2.1 ± 0.3 kbar (range: 1.9–2.6 kbar) for the La Soledad quartz-diorite (Tables S1 and S2).

Al-in-amphibole pressure estimates obtained for rim compositions in contact with plagioclase were also low, being 3.2 ± 0.2 kbar (range: 3.0–3.7 kbar) in the quartz-diorite and 2.9 ± 0.2 kbar (range: 2.5–3.2 kbar) in the mafic enclave from the Guasayán pluton. Lower pressure values of 1.6 ± 0.04 kbar (range: 1.5–1.6 kbar) have been obtained for the mafic enclave of the El Escondido pluton.

The amphibole-plagioclase barometer from [21] gave pressure values of 2.3 ± 0.7 kbar (range: 1.5–3.5 kbar) and 2.8 ± 0.9 kbar (range: 1.7–4.1 kbar) for core and rim compositions in the mafic enclave of the Guasayán pluton; and 1.0 ± 0.5 kbar (range: 0.6–2.0 kbar) for core compositions on the mafic enclave from the El Escondido pluton, whereas unrealistic negative values were obtained for rim compositions of this sample. It is worth noting that the obtained pressure values for the enclave of the Guasayán pluton are equivalent to those obtained with the Al-in-amphibole barometer for this rock.

6.2. Temperature Estimations

Temperatures were only calculated in those samples with amphibole in their major mineral assemblage (GUA 32032, GUA 32030, and GUA 23026). Amphibole-plagioclase temperatures were calculated at 3 kbar for the La Soledad quartz-diorite and the enclave of the Guasayán pluton and 2 kbar for the enclave of the El Escondido pluton. It should be noted that the obtained temperatures with the Ti-Amphibole thermometer and the amphibole-plagioclase thermometer of Holland and Blundy [16] are similar in the case of the La Soledad quartz-diorite and the mafic enclave from the Guasayán pluton (Tables S1 and S2).

For the La Soledad quartz-diorite, we have obtained temperatures ranging between 708 and 878 °C (core: 843 ± 26 °C; rim: 738 ± 30 °C) with the Ti-Amphibole thermometer and between 699 °C and 857 °C (core: 814 ± 25 °C; rim: 742 ± 18 °C) with amphibole-plagioclase expression A of Holland and Blundy [16].

For the enclave from the Guasayán pluton, the calculated temperatures varied from 721 to 845 °C (core: 831 ± 13 °C; rim: 771 ± 23 °C) and from 744 to 860 °C (core: 835 ± 20 °C; rim: 794 ± 28 °C) with the Ti-Amphibole thermometer and the amphibole-plagioclase thermometer of Holland and Blundy [16], respectively.

Finally, for the enclave from the El Escondido pluton we have obtained temperatures of 646 ± 29 °C (Ti-Amphibole thermometer), 733 ± 18 °C (Holland and Blundy's thermometer), and 696 ± 21 °C (expressions A1, A2, and B2 from Molina et al. [22]) for core compositions, and temperatures of 418–589 °C (Ti-Amphibole thermometer), 643 ± 8 °C (Holland and Blundy's thermometer), and 624 ± 7 °C (expressions A1, A2, and B2 from Molina et al. [22]) for rim compositions. The lower temperatures and pressures obtained for this sample are consistent with the subsolidus reequilibration likely experienced by this rock, as indicated in Section 5.3 (Figure 5B). Consequently, only the temperatures obtained for core compositions will be considered for estimating the crystallization conditions.

6.3. fO_2 Estimations

The oxygen fugacity conditions of these rocks were established using Fe/(Fe + Mg) ratios of amphibole and biotite. Fe/(Fe + Mg) ratios of amphibole range from 0.43 to 0.57 and indicate high oxidizing conditions (Figura 7A) for the La Soledad quartz-diorite and the mafic enclaves. Fe/(Fe + Mg) ratios of biotite vary between 0.46 and 0.66, suggesting that all these granitoids crystallized under oxygen fugacity conditions between QFM + 1 and QFM + 2 (Figure 7B), which are coherent with the oxidizing conditions inferred from amphibole compositions.

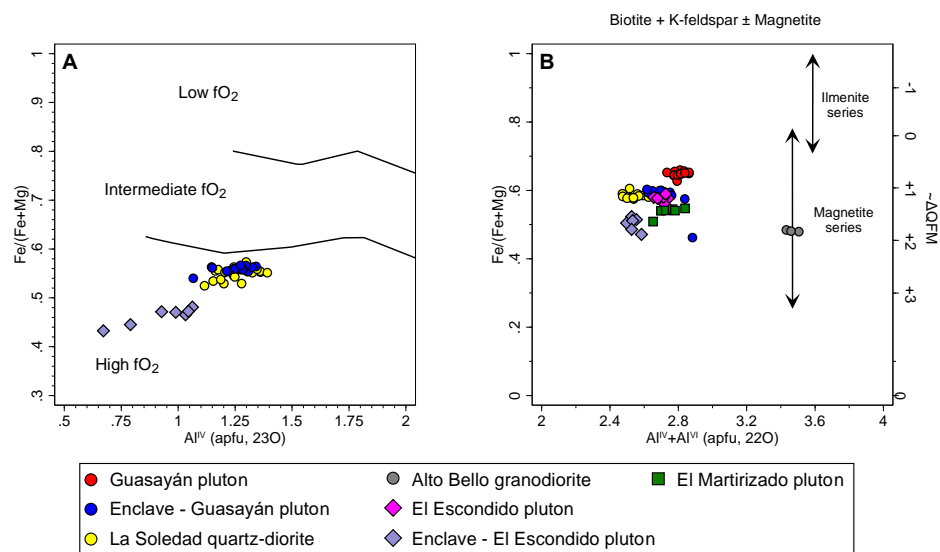


Figure 7. Oxygen fugacity estimation for the granitoids from the Sierra de Guasayán. (A) Fe/(Fe + Mg) vs. Al^{IV} diagram for amphibole. Compositional fields after [25] (B) Fe/(Fe + Mg) vs. Al^{IV} + Al^{VI} for biotite. Ilmenite and magnetite series after [27].

7. Discussion

7.1. Crystallization Conditions

The crystallization conditions (P , T , and fO_2) of the granitoids from the Sierra de Guasayán were constrained on the basis of the compositions of biotite, titanite, amphibole, and plagioclase. P - T conditions were calculated for all granitoids (Tables S1 and S2) except for the Alto Bello granodiorite whose strongly peraluminous character ($ASI = 1.49$ and presence of biotite, muscovite, cordierite, and sillimanite) prevented the use of the total Al-in-biotite barometer, since it was calibrated for metaluminous to slightly peraluminous granites [17].

Pressure estimations obtained with the biotite and titanite barometers are similar (1.0–2.1 and 1.6–2.8 kbar, respectively) and indicate low crystallization pressures for all the studied samples. These low P crystallization conditions are also supported by the Al-in-amphibole barometer with pressure values around 3 kbar for the La Soledad quartz-diorite and the mafic enclave from the Guasayán pluton. The pressures obtained from the amphibole compositions are higher than those obtained from the biotite compositions of the same sample (see Section 6.1 and Table S2), which may suggest that amphibole crystallized earlier than biotite as indicated by the presence of scarce amphibole inclusions in biotite from the La Soledad quartz-diorite. Furthermore, the low accuracy of the biotite barometer should also be considered (Figure 8 in [17]). Pressure obtained with the amphibole-plagioclase barometer for the mafic enclave from the Guasayán pluton is more variable but still equivalent to that obtained with the Al-in-amphibole barometer, with low values around 2.5 kbar.

Ti-in-Amphibole and amphibole-plagioclase temperatures indicate that crystallization of amphibole could have started at around 830 °C and continued to temperatures close to 740 °C in the quartz-diorite and close to 770 °C in the enclave from the Guasayán pluton. On the other hand, although the amphibole in the enclave of the El Escondido pluton seems to have undergone subsolidus reequilibration as evidenced by its lower P - T estimations and low Ti contents ($TiO_2 < 1$ wt.%), it might have crystallized at temperatures around 700 °C or higher.

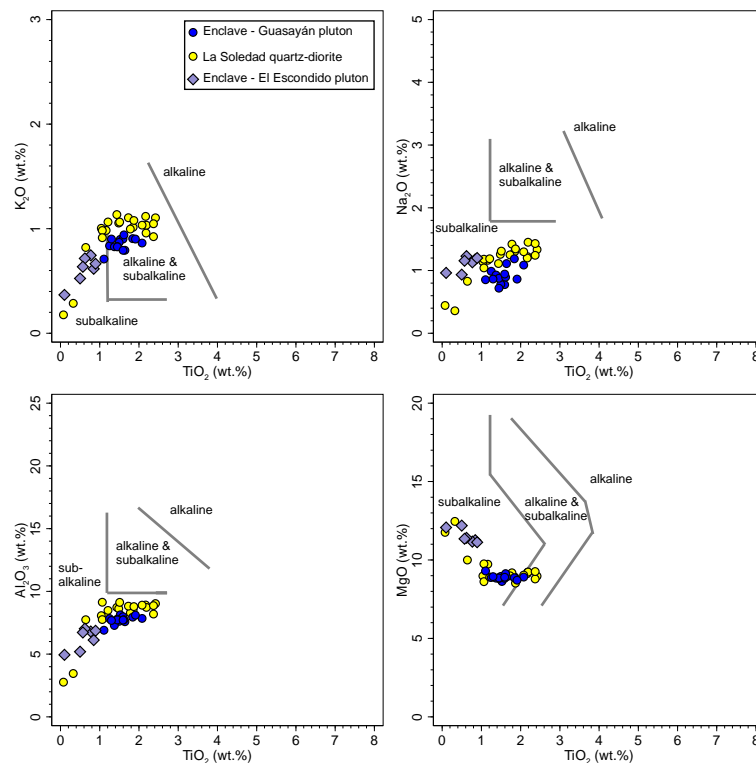


Figure 8. Composition of amphiboles from the granitoids of the Sierra de Guasayán. MgO vs. TiO_2 , Na_2O vs. TiO_2 , K_2O vs. TiO_2 and Al_2O_3 vs. TiO_2 diagrams. Alkaline to subalkaline fields after [14].

$\text{Fe}/(\text{Fe} + \text{Mg})$ ratios of biotite (0.46–0.66) and amphibole (0.43–0.57) from the studied granitoids indicate that these rocks crystallized under oxidizing conditions (Figure 7A,B) with oxygen fugacity conditions between QFM + 1 and QFM + 2 (Figure 7B), showing $\text{Fe}/(\text{Fe} + \text{Mg})$ ratios typical of rocks of the magnetite series (Figure 7B; [27]). This is coherent with the presence of magnetite in most of the samples. Interestingly, the lower $\text{Fe}/(\text{Fe} + \text{Mg})$ ratios of amphibole and biotite from the mafic enclave of the El Escondido pluton (Figure 7) suggest it crystallized under the most oxidizing conditions, which could also be related to the subsolidus alteration experienced by the enclave.

Consequently, the granitoids from the Sierra de Guasayán were emplaced under oxidizing conditions, low-pressure (<3 kbar), and temperatures mostly lower than 770 °C. These shallow emplacement conditions are consistent with the development of hornfels with biotite + plagioclase + K-feldspar + quartz and poikilitic cordierite porphyroblasts, since this mineral assemblage is typical of low-pressure conditions [75]. Furthermore, similar emplacement conditions with pressures lower than 3 kbar and temperatures ranging between 674 and 815 °C have been reported for Cambrian granitoids and subvolcanic rocks from the Sierra Norte-Ambargasta batholith ([76,77] and references therein), for which contact metamorphism conditions with pressure also lower than 3 kbar and temperatures between 530 and 670 °C has been determined (e.g., [78,79]). Accordingly, the Cambrian granitic magmatism from the Sierra de Guasayán and the Sierra Norte-Ambargasta batholith represents shallow structural levels (<12 km) of the Pampean magmatic arc.

7.2. Mineralogical Characterization and Petrogenetic Implications

The Chemical composition of granitoids is commonly reflected in their petrographic and mineralogical characteristics. For instance, many of the mineralogical differences between the I- and S-type granites are linked to the differences in chemical composition between the two groups [5]. In addition, numerous studies have highlighted that the chemical composition of minerals largely corresponds to the nature and crystallizing conditions of the magma from which they crystallized (e.g., [9–14,73]). In this regard,

differences in the major mineral assemblage among the studied granitoids could also be attributed to variations in their whole-rock compositions and ultimately to differences in their sources and petrogenetic processes.

Regarding mineral assemblages, the granitoids from the Sierra de Guasayán could be divided into: (1) those with a clear calc-alkaline I-type affinity such as the La Soledad quartz-diorite (amphibole, biotite, and titanite) and the mafic enclaves from the Guasayán and El Escondido plutons (biotite, amphibole, and epidote \pm allanite); (2) those with a likely but less evident I-type nature such as the Guasayán, El Escondido and El Martirizado plutons with biotite, monazite, and magnetite as distinctive minerals; and (3) the Alto Bello two mica granodiorite with an obvious S-type affinity (biotite, muscovite, cordierite, sillimanite, and monazite).

Chemical compositions of amphibole and biotite supported this subdivision based on the different mineral assemblages. Amphiboles from the quartz-diorite and the mafic enclaves show TiO_2 , MgO , Na_2O , K_2O , and Al_2O_3 contents typical of subalkaline and transitional magmas (Figure 8), in accordance with their calc-alkaline nature. This is also supported by biotite compositions (Figure 9), which plotted in the field of biotite from calc-alkaline granitoids in the discrimination diagrams of Abdel-Rahman [12] and in the subalkaline compositional field of the diagram from Nachit et al. [11]. Compositions of biotite from the Alto Bello granodiorite are notably consistent with an S-type affinity, since these biotites show high Al contents (Figure 9; Table S1), classifying thus as siderophyllite to high-Al annite and plotting in the field of biotites from peraluminous granitoids (Figure 9). On the other hand, biotites from the El Escondido and El Martirizado plutons have typical compositions of biotites from calc-alkaline granites (Figure 9), supporting thus an I-type affinity. However, biotites from the Guasayán pluton present more ambiguous compositions since they plot indistinctly as calc-alkaline and peraluminous granitoids straddling the boundary between both compositional fields in the diagrams of Abdel-Rahman [12] (Figure 9A–C), and in the field of subalkaline granites of the diagram of Nachit et al. [11] (Figure 9D). This could indicate a hybrid or transitional nature for the Guasayán pluton.

Available whole-rock compositions for the La Soledad quartz-diorite (metaluminous, calc-alkalic, and magnesian) and the Alto Bello granodiorite (strongly peraluminous, calc-alkalic, and magnesian) [56] are consistent with the mineralogical characteristics discussed above, allowing its classification as I-type and S-type granitoids, respectively. There is no published whole-rock composition for the El Martirizado pluton, but its mineral assemblage along with the biotite chemistry suggests a calc-alkaline I-type affinity. In the case of the Guasayán and El Escondido plutons, although their whole-rock composition (slightly peraluminous, calc-alkalic, and magnesian) [43,56] and mineralogical characteristics point to a likely I-type affinity, they could not be easily classified because they lack hornblende and titanite, and their peraluminosity (ASI: 1.05–1.1) is relatively high for such intermediate compositions (SiO_2 range: 64.7–69.2 wt.%) that would be more expected in more evolved I-type granites ($\text{SiO}_2 > 70$ wt.%) [80]. This is also highlighted by the ambiguous compositions (calc-alkaline and peraluminous affinities) shown by biotite from the Guasayán pluton (Figure 9), but less so by the biotite from the El Escondido pluton, which has typical compositions of I-type granites (Figure 9). Therefore, at least granitoids from the Guasayán pluton could be better classified as hybrid or transitional I-S-type granites. This can also be extended to the El Escondido pluton, since it has a similar mineral assemblage and whole-rock composition to those of the Guasayán pluton, and both plutons also have abundant mafic enclaves and rapakivi texture (Figure 3). The hybrid nature of the Guasayán pluton agrees with zircon Hf-isotope data for a biotite granodiorite from the northern sector of the pluton (ϵHf_i ranging from -4.76 to -0.12) [43], suggesting an interaction between juvenile and anatectic sources, with a predominance of the latter, or alternatively a heterogeneous source (see discussion in [43]). Although, this latter can be discarded by the mafic enclaves and rapakivi texture that are evidence for hybridization (e.g., [81]).

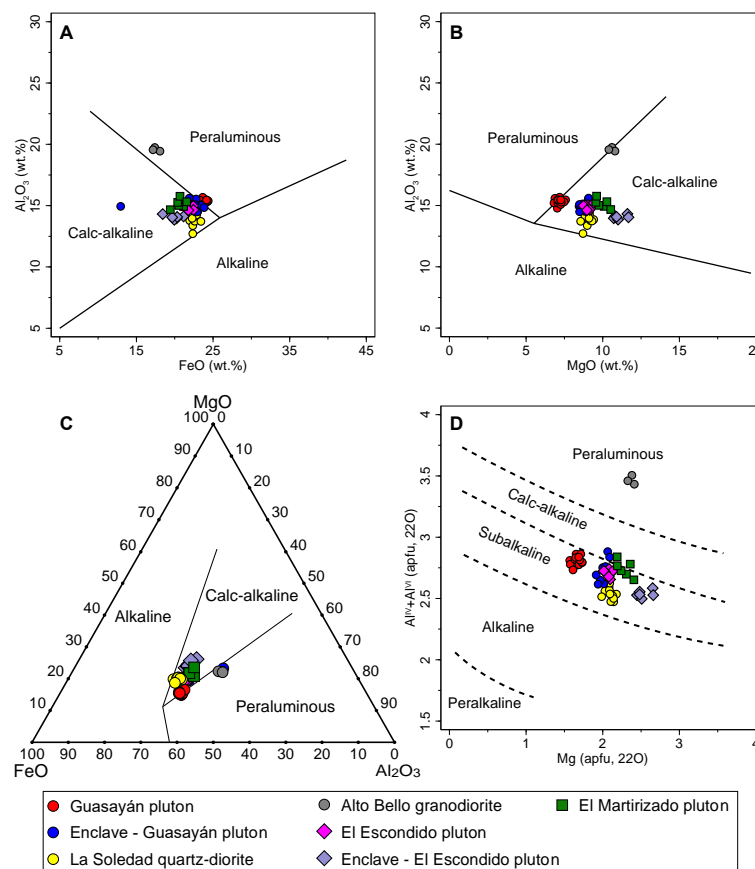


Figure 9. Composition of biotites from the granitoids of the Sierra de Guasayán. Al_2O_3 vs. FeO (A), Al_2O_3 vs. MgO (B) and MgO – FeO – Al_2O_3 (C) discrimination diagrams (after [12]) and $Al^{IV} + Al^{VI}$ vs. Mg diagram (D) (after [11]).

Available zircon Hf-isotope data for early Cambrian granitoids from the Tastil batholith, the Sierra Norte-Ambargasta batholith, and the North Patagonian Massif show ϵHf_i values between -6.9 and $+1.5$ [40,82], matching those from the Guasayan pluton and also suggesting analogous processes participate in the genesis of these magmas. Similar processes involving hybridization that could have been accompanied by assimilation of the metamorphic basement have been invoked to explain the geochemistry of the equivalent granitoids from the Sierra Norte-Ambargasta batholith [41,77]. This is also supported by the abundance of mafic microgranular enclaves and the existence of disequilibrium textures (such as rapakivi texture and reverse zoning in plagioclase) recognized in the granitoids from the Sierra Norte-Ambargasta batholith ([77] and references therein), i.e., similar to what is observed in the Guasayán and El Escondido plutons. All of this seems to indicate that hybridization processes could play an important role in the generation of magmas during the Pampean Orogeny.

8. Conclusions

The combined study of mineral assemblages, textural evidence, and mineral chemistry with the available geochemical and isotope data for the granitoids from the Sierra the Guasayán allow us to subdivide them into three groups with distinctive characteristics:

1. I-type granitoids: La Soledad quartz-diorite, the mafic enclaves from the Guasayán and El Escondido plutons and likely the El Martirizado pluton.
2. S-type granitoid: The Alto Bello granodiorite.
3. Hybrid or transitional I-S-type granitoids that represent the most voluminous magmatism in the region: The Guasayán and El Escondido plutons.

The obtained *P-T* crystallization conditions suggest that these magmas were emplaced at shallow structural levels (<3 kbar), under oxidizing conditions and temperatures lower than 770 °C. These conditions seem to be common to granitoids formed in the Pampean magmatic arc (e.g., granites from the Sierra Norte-Ambargasta batholith).

Furthermore, the hybrid nature of the Guasayán and El Escondido plutons highlighted here is similar to that reported for other granites of the Pampean magmatic arc, suggesting therefore that magma mixing processes could have played an important role in the genesis of granitoids magmas during the Pampean Orogeny.

Supplementary Materials: The following are available online at <https://www.mdpi.com/2075-163X/11/2/166/s1>, Table S1: mineral chemistry of feldspars, amphiboles, micas, and titanite from the granitoids of the Sierra de Guasayán, Table S2: Summary of *P-T* conditions in mineral assemblages from the granitoids of the Sierra de Guasayán.

Author Contributions: Conceptualization, P.S.Z. and J.A.M.; methodology, P.S.Z., J.A.M., and S.O.V.; formal analysis, S.O.V.; investigation, P.S.Z., J.A.M., S.O.V., E.G.B., J.A.D., M.M.M.C., C.B., M.B., S.S.-V., and C.I.L.W.; resources, E.G.B.; data curation, P.S.Z. and J.A.M.; writing—original draft preparation, P.S.Z. and J.A.M.; writing—review and editing, P.S.Z., J.A.M., S.O.V., E.G.B., J.A.D., M.M.M.C., C.B., M.B., S.S.-V., and C.I.L.W.; visualization, P.S.Z., J.A.M., and S.O.V.; supervision, S.O.V. and E.G.B.; project administration, E.G.B.; funding acquisition, E.G.B. All authors have read and agreed to the published version of the manuscript.

Funding: This research was funded by FONCyT (grant PICT-2017-0619), SECyT-UNC (grant SECyT-UNC-2018-Consolidar) and CONICET (grant PIP 2015-2018 11220150100901CO).

Institutional Review Board Statement: Not applicable.

Informed Consent Statement: Not applicable.

Data Availability Statement: The data presented in this study are openly available in [Supplementary Material] at [<https://www.mdpi.com/2075-163X/11/2/166/s1>].

Acknowledgments: We thank anonymous reviewers for the thorough revision of the manuscript and the insightful comments that have greatly improved the quality of this presentation. We also thank Jaroslav Dostal for his efficient editorial handling.

Conflicts of Interest: The authors declare no conflict of interest.

References

1. Frost, B.R.; Barnes, C.G.; Collins, W.J.; Arculus, R.J.; Ellis, D.J.; Frost, C.D. A geochemical classification for granitic rocks. *J. Petrol.* **2001**, *42*, 2033–2048. [[CrossRef](#)]
2. Kemp, A.I.S.; Hawkesworth, C.J. Granitic perspective on the generation and secular evolution of continental crust. *Treatise Geochem.* **2003**, *3*, 349–410. [[CrossRef](#)]
3. Castro, A. The off-crust origin of granite batholiths. *Geosci. Front.* **2014**, *5*, 63–75. [[CrossRef](#)]
4. Bonin, B.; Janoušek, V.; Moyen, J.F. Chemical variation, modal composition and classification of granitoids. *Geol. Soc. Lond. Spec.* **2020**, *491*, 9–51. [[CrossRef](#)]
5. Chappell, B.W.; White, A.J.R. Two contrasting granite types: 25 years later. *Aust. J. Earth Sci.* **2001**, *48*, 489–499. [[CrossRef](#)]
6. Bea, F. Residence of REE, Y, Th and U in granites and crustal protoliths: Implications for the chemistry of crustal melts. *J. Petrol.* **1996**, *37*, 521–552. [[CrossRef](#)]
7. Chappell, B.W. Aluminium saturation in I- and S-type granites and the characterization of fractionated haplogranites. *Lithos* **1999**, *46*, 535–551. [[CrossRef](#)]
8. Miller, C.F. Are strongly peraluminous magmas derived from pelitic sedimentary sources? *J. Geol.* **1985**, *93*, 673–689. [[CrossRef](#)]
9. Neiva, A.M.R. Geochemistry of hybrid granitoid rocks and of their biotites from central northern Portugal and their petrogenesis. *Lithos* **1981**, *14*, 149–163. [[CrossRef](#)]
10. Leterrier, J.; Maury, R.C.; Thonon, P.; Girard, D.; Marchal, M. Clinopyroxene composition as a method of identification of the magmatic affinities of paleo-volcanic series. *Earth Planet. Sci. Lett.* **1982**, *59*, 139–154. [[CrossRef](#)]
11. Nachit, H.; Razafimahefa, N.; Stussi, J.M.; Carron, J.P. Composition chimique des biotites et typologie magmatique des granites. *C.R. Acad. Sci. Paris* **1985**, *301*, 813–818.
12. Abdel-Rahman, A.M. Nature of biotites from alkaline, calc-alkaline, and peraluminous magmas. *J. Petrol.* **1994**, *35*, 525–541. [[CrossRef](#)]

13. Shabani, A.A.T.; Lalonde, A.E.; Whalen, J.B. Composition of biotite from granitic rocks of the Canadian Appalachian orogen: A potential tectonomagmatic indicator? *Can. Min.* **2003**, *41*, 1381–1396. [\[CrossRef\]](#)
14. Molina, J.F.; Searrow, J.H.; Montero, P.; Bea, F. High-Ti amphibole as a petrogenetic indicator of magma chemistry: Evidence for mildly alkalic-hybrid melts during evolution of Variscan basic–ultrabasic magmatism of Central Iberia. *Contrib. Mineral. Petr.* **2009**, *158*, 69–98. [\[CrossRef\]](#)
15. Schmidt, M.W. Amphibole composition in tonalite as a function of pressure: An experimental calibration of the aluminium-in-hornblende. *Contrib. Mineral. Petr.* **1992**, *110*, 304–310. [\[CrossRef\]](#)
16. Holland, T.; Blundy, J. Non-ideal interactions in calcic amphiboles and their bearing on amphibole–plagioclase thermometry. *Contrib. Mineral. Petr.* **1994**, *116*, 433–447. [\[CrossRef\]](#)
17. Uchida, E.; Endo, S.; Makino, M. Relationship between solidification depth of granitic rocks and formation of hydrothermal ore deposits. *Resour. Geol.* **2007**, *57*, 47–56. [\[CrossRef\]](#)
18. Ridolfi, F.; Renzulli, A. Calcic amphiboles in calc-alkaline and alkaline magmas: Thermobarometric and chemometric empirical equations valid up to 1130 °C and 2.2 GPa. *Contrib. Mineral. Petr.* **2012**, *163*, 877–895. [\[CrossRef\]](#)
19. Erdmann, S.; Martel, C.; Pichavant, M.; Kushnir, A. Amphibole as an archivist of magmatic crystallization conditions: Problems, potential, and implications for inferring magma storage prior to the paroxysmal 2010 eruption of Mount Merapi, Indonesia. *Contrib. Mineral. Petrol.* **2014**, *167*, 1016–1038. [\[CrossRef\]](#)
20. Erdmann, S.; Wang, R.C.; Huang, F.F.; Scaillet, B.; Zhao, K.; Liu, H.S.; Chen, Y.; Faure, M. Titanite: A potential solidus barometer for granitic magma systems. *Compt. Rendus Geosci.* **2019**, *351*, 551–561. [\[CrossRef\]](#)
21. Molina, J.F.; Moreno, J.A.; Castro, A.; Rodríguez, C.; Fershtater, G.B. Calcic amphibole thermobarometry in metamorphic and igneous rocks: New calibrations based on plagioclase/amphibole Al–Si partitioning and amphibole/liquid Mg partitioning. *Lithos* **2015**, *232*, 286–305. [\[CrossRef\]](#)
22. Molina, J.F.; Cambeses, A.; Moreno, J.A.; Morales, I.; Montero, P.; Bea, F. A reassessment of the amphibole–plagioclase NaSi–CaAl exchange thermometer with applications to igneous rocks. *Am. Mineral.* **2021**, in press. [\[CrossRef\]](#)
23. Mutch, E.J.F.; Blundy, J.D.; Tattitch, B.C.; Cooper, F.J.; Brooker, R.A. An experimental study of amphibole stability in low-pressure granitic magmas and a revised Al-in-hornblende geobarometer. *Contrib. Mineral. Petr.* **2016**, *171*, 85. [\[CrossRef\]](#)
24. Liao, Y.; Wei, C.; Rehman, H.U. Titanium in calcium amphibole: Behavior and thermometry. *Am. Mineral.* **2021**, in press. [\[CrossRef\]](#)
25. Anderson, J.L.; Smith, D.R. The effects of temperature and fO₂ on the Al-in-hornblende barometer. *Am. Mineral.* **1995**, *80*, 549–559. [\[CrossRef\]](#)
26. Dall’Agnol, R.; Oliveira, D.C. Oxidized, magnetite series, rapakivi-type granites of Carajás, Brazil: Implications for classification and petrogenesis of A-type granites. *Lithos* **2007**, *93*, 215–233. [\[CrossRef\]](#)
27. Anderson, J.L.; Barth, A.P.; Wooden, J.L.; Mazdab, F. Thermometers and thermobarometers in granitic systems. *Rev. Mineral. Geochem.* **2008**, *69*, 121–142. [\[CrossRef\]](#)
28. Ramos, V.A.; Cristallini, E.O.; Pérez, D.J. The Pampean flat-slab of the Central Andes. *J. S. Am. Earth Sci.* **2002**, *15*, 59–78. [\[CrossRef\]](#)
29. Caminos, R. Sierras Pampeanas de Catamarca, Tucumán, La Rioja y San Juan. In *Símpoio de Geología Regional Argentina, No. 2*; Leanza, A.F., Ed.; Academia Nacional de Ciencias de Córdoba: Córdoba, Argentina, 1972; Volume 1, pp. 41–79.
30. Casquet, C.; Baldo, E.G.; Pankhurst, R.J.; Rapela, C.W.; Galindo, C.; Fanning, C.M.; Saavedra, J. Involvement of the Argentine Precordillera terrane in the Famatinian mobile belt: U–Pb SHRIMP and metamorphic evidence from the Sierra de Pie de Palo. *Geology* **2001**, *29*, 703–706. [\[CrossRef\]](#)
31. Sato, A.M.; González, P.D.; Llambías, E.J. Evolución del Orógeno Famatiniano en la Sierra de San Luis: Magmatismo de arco, deformación y metamorfismo de bajo a alto grado. *Rev. Asoc. Geológica Argent.* **2003**, *58*, 487–504.
32. Rapela, C.W.; Pankhurst, R.J.; Casquet, C.; Baldo, E.; Galindo, C.; Fanning, C.M.; Dahlquist, J.A. The Western Sierras Pampeanas: Protracted Grenville history (1330–1030 Ma) of intra-oceanic arcs, subduction-accretion at continental-edge and AMCG intraplate magmatism. *J. S. Am. Earth Sci.* **2010**, *29*, 105–127. [\[CrossRef\]](#)
33. Varela, R.; Basei, M.A.S.; González, P.D.; Sato, A.M.; Naipauer, M.; Campos Neto, M.C.A.; Meira, V.T. Accretion of Grenvillian terranes to the southwestern border of the Río de La Plata craton, western Argentina. *Int. J. Earth Sci.* **2011**, *100*, 243–272. [\[CrossRef\]](#)
34. Dahlquist, J.A.; Alasino, P.H.; Basei, M.A.S.; Morales Cámara, M.; Macchioli Grandre, M.; Campos Neto, M.C. Petrological, geochemical, isotopic, and geochronological constraints for the Late Devonian–Early Carboniferous magmatism in SW Gondwana (27–32° LS): An example of geodynamic switching. *Int. J. Earth Sci.* **2018**, *107*, 2575–2603. [\[CrossRef\]](#)
35. Rapela, C.W.; Verdecchia, S.O.; Casquet, C.; Pankhurst, R.J.; Baldo, E.G.; Galindo, C.; Murra, J.A.; Dahlquist, C.; Mark Fanning, C. Identifying Laurentian and SW Gondwana sources in the Neoproterozoic to Early Paleozoic metasedimentary rocks of the Sierras Pampeanas: Paleogeographic and tectonic implications. *Gondwana Res.* **2016**, *32*, 193–212. [\[CrossRef\]](#)
36. Dahlquist, J.A.; Morales Cámara, M.M.; Alasino, P.; Tickyj, H.; Basei, M.A.S.; Galindo, C.; Moreno, J.A.; Rocher, S. Geochronology and geochemistry of Devonian magmatism in the Frontal Cordillera (Argentina): Geodynamic implications for the pre-Andean SW Gondwana margin. *Int. Geol. Rev.* **2020**, *177*, 455–474. [\[CrossRef\]](#)
37. Rapela, C.W.; Pankhurst, R.J.; Casquet, C.; Dahlquist, J.A.; Fanning, C.M.; Baldo, E.G.; Galindo, C.; Alasino, P.H.; Ramacciotti, C.D.; Verdecchia, S.O.; et al. A review of the Famatinian Ordovician magmatism in southern South America: Evidence of

- lithosphere reworking and continental subduction in the early proto-Andean margin of Gondwana. *Earth Sci. Rev.* **2018**, *187*, 259–285. [\[CrossRef\]](#)
38. Rapela, C.W.; Pankhurst, R.J.; Casquet, C.; Baldo, E.; Saavedra, J.; Galindo, C.; Fanning, C.M. The Pampean orogeny of the south proto-Andes: Evidence for Cambrian continental collision in the Sierras de Córdoba. In *The Proto-Andean Margin of Gondwana*; Pankhurst, R.J., Rapela, C.W., Eds.; Geological Society, London, Special Publications: London, UK, 1998; Volume 142, pp. 181–217. [\[CrossRef\]](#)
 39. Omarini, R.H.; Sureda, R.J.; López de Azarevich, V.L.; Hauser, N. El basamento Neoproterozoico- Cámbrico inferior en la provincia de Jujuy. In *Relatorio del Congreso Geológico Argentino. Geología y Recursos Naturales de la Provincia de Jujuy*, No. 17; Coira, B., Zappettini, E., Eds.; Buenos Aires Asociación Geológica Argentina: San Salvador de Jujuy, Argentina, 2008; pp. 17–28.
 40. Hauser, N.; Matteini, M.; Omarini, R.; Pimentel, M. Combined U-Pb and Lu-Hf isotope data on turbidites of the Paleozoic basement of NW Argentina and petrology of associated igneous rocks: Implications for the tectonic evolution of western Gondwana between 560 and 460 Ma. *Gondwana Res.* **2011**, *19*, 100–127. [\[CrossRef\]](#)
 41. Iannizzotto, N.F.; Rapela, C.W.; Baldo, E.G.A.; Galindo, C.; Fanning, C.M.; Pankhurst, R.J. The Sierra Norte-Ambargasta batholith: Late Ediacaran-Early Cambrian magmatism associated with Pampean transpressional tectonics. *J. S. Am. Earth Sci.* **2013**, *42*, 127–143. [\[CrossRef\]](#)
 42. Von Gosen, W.; McClelland, W.C.; Loske, W.; Martínez, J.C.; Prozzi, C. Geochronology of igneous rocks in the Sierra Norte de Córdoba (Argentina): Implications for the Pampean evolution at the western Gondwana margin. *Lithosphere* **2014**, *6*, 277–300. [\[CrossRef\]](#)
 43. Dahlquist, J.A.; Verdecchia, S.O.; Baldo, E.G.; Basei, M.A.S.; Alasino, P.H.; Uran, G.A.; Rapela, C.W.; Da Costa Campos Neto, M.; Zandomeni, P.S. Early Cambrian U-Pb zircon age and Hf-isotope data from the Guasayán pluton, Sierras Pampeanas, Argentina: Implications for the northwestern boundary of the Pampean arc. *Andean Geol.* **2016**, *43*, 137–150. [\[CrossRef\]](#)
 44. Casquet, C.; Dahlquist, J.A.; Verdecchia, S.O.; Baldo, E.G.; Galindo, C.; Rapela, C.W.; Pankhurst, R.J.; Morales, M.M.; Murra, J.A.; Fanning, C.M. Review of the Cambrian Pampean orogeny of Argentina; a displaced orogeny formerly attached to the Saldania Belt of South Africa? *Earth Sci. Rev.* **2018**, *177*, 209–225. [\[CrossRef\]](#)
 45. Cawood, P.A. Terra Australis Orogen: Rodinia breakup and development of the Pacific and Iapetus margins of Gondwana during the Neoproterozoic and Paleozoic. *Earth Sci. Rev.* **2005**, *69*, 249–279. [\[CrossRef\]](#)
 46. Beder, R. La Sierra de Guasayán y sus alrededores. *Dir. Gen. Minas Geol. Hidrogeol.* **1928**, *39*, 171.
 47. González, R.R.; Toselli, A.J. Radiometric dating of igneous rocks from Sierras Pampeanas, Argentina. *Rev. Bras. Geocienc.* **1974**, *4*, 137–141. [\[CrossRef\]](#)
 48. Battaglia, A. *Descripción geológica de las Hojas 13f, Río Hondo 13g Santiago del Estero; 14g, El Alto; 14h, Villa San Martín; 15g, Frías (provincias de Santiago del Estero, Catamarca y Tucumán)*; Boletín 186; Instituto de Geología y Recursos Minerales, Servicio Geológico Minero Argentino: Buenos Aires, Argentina, 1982; p. 80.
 49. Omil, M. Geología y Geomorfología del Basamento de la Sierra de Guasayán, Provincia de Santiago del Estero. Ph.D. Thesis, Universidad Nacional de Tucumán, Tucumán, Argentina, 1992.
 50. Blasco, G.; Caminos, R.L.; Lapido, O.; Lizuaín, A.; Martínez, H.; Nullo, F.; Panza, J.L.; Sacomani, L. *Hoja Geológica 2966-II, San Fernando del Valle de Catamarca, Provincias de Catamarca, Santiago del Estero y Tucumán*; Boletín 212; Instituto de Geología y Recursos Minerales, Servicio Geológico Minero Argentino: Buenos Aires, Argentina, 1994; p. 50.
 51. Dal Molin, C.; Fernández, D.; Escosteguy, L.; Villegas, D.; González, O.; Martínez, L. *Hoja geológica 2766-IV, Concepción, Provincias de Tucumán, Catamarca y Santiago del Estero*; Boletín 324; Instituto de Geología y Recursos Minerales, Servicio Geológico Minero Argentino: Buenos Aires, Argentina, 2003; p. 41.
 52. Von Gosen, W.; Buggisch, W.Y.; Prozzi, C. Provenance and geotectonic setting of Late Proterozoic—Early Cambrian metasediments in the Sierras de Córdoba and Guasayán (western Argentina): A geochemical approach. *Neues Jahrb. Geol. Palaontol. Abh.* **2009**, *251*, 257–284. [\[CrossRef\]](#)
 53. Turner, J.C.M. *Estratigrafía de la Sierra de Santa Victoria y Adyacencias*; Boletín 41; Academia Nacional de Ciencias Córdoba: Córdoba, Argentina, 1960; pp. 163–196.
 54. Omarini, R.H.; Sureda, R.; Toselli, A.J.; Rossi, J.N. Ciclo Pampeano-Proterozoico superior-Eocámbrico: Magmatismo. In *Relatorio del Congreso Geológico Argentino*, No. 14; González Bonorino, G., Omarini, R., Viramonate, J., Eds.; Actas Tomo I: Salta, Argentina, 1999; pp. 29–40.
 55. Escayola, M.P.; van Staal, C.R.; Davis, W.J. The age and tectonic setting of the Puncoviscana Formation in northwestern Argentina: An accretionary complex related to Early Cambrian closure of the Puncoviscana Ocean and accretion of the Arequipa-Antofalla block. *J. S. Am. Earth Sci.* **2011**, *32*, 438–459. [\[CrossRef\]](#)
 56. Zandomeni, P.S.; Verdecchia, S.O.; Baldo, E.G.; Dahlquist, J.A.; Uran, G.M.; Alasino, P.H. *El magmatismo Cámbrico de la Sierra de Guasayán (Provincia de Santiago del Estero) y su Vinculación a la Orogenia Pampeana*; Capítulo del Relatorio del XX Congreso Geológico Argentino: Tucumán, Argentina, 2017; pp. 308–322.
 57. Lira, R.; Millone, H.A.; Kirschbaum, A.M.; Moreno, R.S. Calc-alkaline arc granitoid activity in the Sierra Norte-Ambargasta Ranges, Central Argentina. *J. S. Am. Earth Sci.* **1997**, *10*, 157–177. [\[CrossRef\]](#)
 58. Whitney, D.L.; Evans, B.W. Abbreviations for names of rock-forming minerals. *Am. Mineral.* **2010**, *95*, 185–187. [\[CrossRef\]](#)
 59. Papike, J.J. Chemistry of the rock-forming silicates: Ortho, ring, and single-chain structures. *Rev. Geophys.* **1987**, *25*, 1483–1526. [\[CrossRef\]](#)

-
60. Papike, J.J. Chemistry of the rock-forming silicates: Multiple-chain, sheet, and framework structures. *Rev. Geophys.* **1988**, *26*, 407–444. [[CrossRef](#)]
 61. Deer, W.A.; Howie, R.A.; Zussman, J. *An Introduction to the Rock-Forming Minerals*, 3rd ed.; The Mineralogical Society: London, UK, 2013; pp. 474–475. [[CrossRef](#)]
 62. Rieder, M.; Cavazzini, G.; D'yakonov, Y.; Frank-Kamenetskii, V.; Gottardi, G.; Guggenheim, S.; Koval, P.; Muller, G.; Neiva, A.; Radoslovich, E.; et al. Nomenclature of the micas. *Mineral. Mag.* **1999**, *63*, 267–279. [[CrossRef](#)]
 63. Smith, J.V.; Brown, W.L. Feldspar Minerals. In *Feldspar Minerals*; Springer: Berlin/Heidelberg, Germany, 1988; Volume 1, pp. 1–646.
 64. Locock, A.J. An Excel spreadsheet 869 to classify chemical analyses of amphiboles following the IMA 2012 recommendations. *Comput. Geosci.* **2014**, *62*, 1–11. [[CrossRef](#)]
 65. Hawthorne, F.C.; Oberti, R.; Harlow, G.E.; Maresch, W.V.; Martin, R.F.; Schumacher, J.C.; Welch, M.D. Nomenclature of the amphibole supergroup. *Am. Mineral.* **2012**, *97*, 2031–2048. [[CrossRef](#)]
 66. Robinson, P.; Spear, F.S.; Schumacher, J.C.; Laird, J.; Klein, C.; Evans, B.W.; Doolan, B.L. Phase relations of metamorphic amphiboles: Natural occurrence and theory. *Rev. Mineral.* **1982**, *9B*, 1–227.
 67. Dale, J.; Powell, R.; White, L.; Elmer, F.L.; Holland, T.J.B. A thermodynamic model for Ca–Na–amphiboles in Na₂O–CaO–FeO–MgO–Al₂O₃–SiO₂–H₂O–O for petrological calculations. *J. Metamorph. Geol.* **2005**, *23*, 771–791. [[CrossRef](#)]
 68. Pe-Piper, G. Calcic amphiboles of mafic rocks of the Jefferes Brooks plutonic complex, Nova Scotia, Canada. *Am. Mineral.* **1988**, *73*, 993–1006.
 69. Campos, T.F.C.; Neiva, A.M.R.; Naredi, L.V.S.; Pereira, L.S.; Bonzanini, L.F.; Petta, R.A.; Meyer, F.M. Magmatic Epidote and Amphibole from the Rio Espinharas Hybrid Complex, Northeastern Brazil. *Pesqui. Geociências* **2005**, *32*, 41–55. [[CrossRef](#)]
 70. Tischendorf, G.; Rieder, M.; Förster, H.-J.; Gottesmann, B.; Guidotti, C.V. A new graphical presentation and subdivision of potassium micas. *Mineral. Mag.* **2004**, *68*, 649–667. [[CrossRef](#)]
 71. Tischendorf, G.; Förster, H.-J.; Gottesmann, B.; Rieder, M. True and brittle micas: Composition and solid-solution series. *Mineral. Mag.* **2007**, *71*, 285–320. [[CrossRef](#)]
 72. Nachit, H.; Ibhi, A.; Abia, E.H.; Ohoud, M.B. Discrimination between primary magmatic biotites, reequilibrated biotites and neoformed biotites. *Comptes Rendus Geosci.* **2005**, *337*, 1415–1420. [[CrossRef](#)]
 73. Miller, C.F.; Stoddard, E.F.; Bradfish, L.J.; Dollase, W.A. Composition of plutonic muscovite: Genetic implications. *Can. Mineral.* **1981**, *19*, 25–34.
 74. Kowallis, B.J.; Christiansen, E.H.; Griffen, D.T. Compositional variations in titanite. *Geol. Soc. Am. Abstr. Programs* **1997**, *29*, 402.
 75. Brown, M. Unpairing metamorphic belts: P–T paths and a tectonic model for the Ryoke Belt, southwest Japan. *J. Metamorph. Geol.* **1998**, *16*, 3–12. [[CrossRef](#)]
 76. Poklepovic, M.F.; Lira, R.; Dorais, M.; Millone, H.A. *Consideraciones Geobarométricas de los Granitoides Calco-Alcalinos del Batolito de Sierra Norte-Ambargasta, Córdoba, Argentina*; 16° Congreso Geológico Argentino: La Plata, Argentina, 2005; Volume 1, pp. 619–626.
 77. Lira, R.; Poklepovic, M.F.; O'Leary, M.S. El magmatismo cámbrico en el batolito de Sierra Norte-Ambargasta. In *Geología y Recursos Naturales de la Provincia de Córdoba*; Martino, R., Guerreschi, A., Eds.; Asociación Geológica Argentina: Córdoba, Argentina, 2014; pp. 183–216.
 78. Guerreschi, A.B.; Martino, R.D. *Evolución textural de las corneanas de La Clemira, Sierra de Ambargasta, Santiago del Estero, Argentina*; Actas 2; 15° Congreso Geológico Argentino: El Calafate (Santa Cruz), Argentina, 2002; pp. 180–183.
 79. O'Leary, M.S. Petrología, Geoquímica y Metalogénesis de los Diques Dacítico-Riolíticos del Arco Magmático Cambro-Ordovícico de la Sierra Norte-Ambargasta, Provincias de Córdoba y Santiago del Estero. Ph.D. Thesis, Facultad de Ciencias Exactas, Físicas y Naturales, Universidad Nacional de Córdoba, Córdoba, Argentina, 2004.
 80. Chappell, B.W.; Bryant, C.J.; Wyborn, D. Peraluminous I-type granites. *Lithos* **2012**, *153*, 142–153. [[CrossRef](#)]
 81. Molina, J.F.; Montero, P.; Bea, F.; Scarrow, J.H. Anomalous xenocryst dispersion during tonalite–granodiorite crystal mush hybridization in the midcrust: Mineralogical and geochemical evidence from Variscan appinites (Avila Batholith, Central Iberia). *Lithos* **2012**, *153*, 224–242. [[CrossRef](#)]
 82. Rapela, C.W.; Pankhurst, R.J. The Continental crust of Northeastern Patagonia. *Ameghiniana* **2020**, *57*, 480–498. [[CrossRef](#)]